Zirconium Coordination Chemistry and its Role in Optimizing Hydroxymate Chelation: Insights from Molecular Dynamics

Giulia Sormani,[†] Aruna Korde,[‡] Alex Rodriguez,[¶] Melissa Denecke,[‡] and Ali Hassanali[*,†]

†*The "Abdus Salam" International Centre for Theoretical Physics, I-34151 Trieste, Italy*

‡*International Atomic Energy Agency, A-1400 Vienna, Austria.*

¶*University of Trieste, Trieste, Italy.*

E-mail: ahassana@ictp.it

Abstract

In the last decade, there has been a growth in using Zirconium-89 (^{89}Zr) as a radionuclide in nuclear medicine for cancer diagnostic imaging and drug discovery processes. One of the most popular chelators for ^{89}Zr, is desferrioxamine (DFO) which acts as a hexadentate ligand. The coordination structure of the Zr^{4+}-DFO complex has primarily been informed by DFT-based calculations which typically ignore temperature and therefore entropic and dynamic solvent effects. In this work, free energy calculations using molecular dynamics simulations, where the conformational fluctuations of both the ligand and the solvent are explicitly included, are used to compare the binding of Zr^{4+} cation with two different chelators, DFO and 4HMS, the latter of which has been recently proposed as a better chelator.[1] We find that thermal induced disorder leads an open hexadentate chelate structure of Zr^{4+}-DFO complex, leaving the Zr^{4+} metal exposed to the solvent. A stable coordination of Zr^{4+} with 4HMS, however, is formed involving both hydroxamate groups and water molecules in a more closely packed structure.

Introduction

Nuclear medicine imaging plays an important role in new drug developments, both at preclinical and early clinical stages.[2] Presently, fluorine-18(^{18}F), and gallium-68(^{68}Ga) are the most used positron emission tomography(PET) radionuclides for molecular imaging studies in nuclear medicine.[3] PET permits non-invasive localization and quantification with relatively small amounts of radioactivity, due to its high inherent sensitivity. The short half-lives of both these radionuclides (110 and 68 minutes, respectively), however, pose limitations for imaging biochemical processes with slow pharmacokinetics, such as localization of macromolecules at targeted tissues in macromolecular-based (e.g. antibodies) cancer therapies.[4] On the other hand, Zirconium-89 (^{89}Zr) is suitable for radiolabelling and in-vivo visualization of such processes due to its relatively long half-life (78.4h), which matches the slow

pharmacokinetics of macromolecular therapeutics.[5]

Most emerging therapeutics are based on macromolecules rather than small organic moieties, especially macromolecules that specifically target cancer cells through monoclonal antibodies, cell tracking agents, nucleotides and nanoparticle systems. Nearly 115 clinical studies are currently ongoing with ^{89}Zr labelled molecules.[6] Zirconium-89 can be produced in medium energy medical cyclotrons through the ^{89}Y(p,n) ^{89}Zr nuclear reaction.[7] An ongoing International Atomic Energy Agency (IAEA) co-ordinated research project focuses on standardization of ^{89}Zr production procedures and quality control.[8] Designing a radiopharmaceutical to transfer the radionuclide (such as ^{89}Zr) to specific cells and retain it there for a desire time, with minimum accumulation and faster clearance from other non-target tissues, is a challenging process.

Chelating molecules in radiopharmaceutical design play an important role as anchors for radionuclide metals and for targeting vector macromolecules. In the case of ^{89}Zr, the bacteria-produced siderophore desferrioxamine B (DFO) is most used for radiolabeling.[9,10] DFO is an open-chain, hexadentate chelate molecule having three hydroxamate groups as radiometal binding moieties and a terminal primary amine that allows conjugation with vector biomolecules. In 1964, Baroncelli et al. found a high affinity of Zr^{4+} ions towards hydroxamic acid groups and in 1992, Meijs et al. reported successful radiolabeling of DFO with ^{89}Zr and good in vitro stability of the resulting complex.[11] Since then, many other DFO analogues[12] and other chelators, including acyclic and cyclic polyazacarboxylates,[13,14] have been studied in search of complexes which are more stable in vivo and avoid unspecific uptake of ^{89}Zr in, for example, the bones.[15,16] More recently over the last decade, the speciation and thermodynamic stability of Zr^{4+}-DFO complexes in solution has been investigated through potentiometric, spectrophotometric and mass spectrometry measurements.[17–20] These studies have pointed to the possibility of the formation of non-mononuclear complexes involving DFO and Zr^{4+}.

To streamline and guide such trial-and-error optimization efforts for chelator design, com-

putational methods offer insight into the structure and thermodynamic stability of different chelates under varying conditions mimicking complex biological systems. In this regard, several computational studies have been conducted in order to understand the chelating mechanism of DFO. Specifically, the coordination structure of Zr^{4+} with DFO has been discussed as an important parameter in possibly controlling its stability in vivo. Quantum chemistry-based calculations using Density Functional Theory (DFT) for example, have shown that seven[21] or eight-coordinated[17,22] complexes, with Zr^{4+} bound to the six oxygen atoms of DFO and to one or two oxygen atoms from surrounding water molecules, are found to be the most stable complexes. While DFT approaches are more accurate in-so-far as including electronic effects, the vast majority of theoretical studies of DFO and Zr^{4+} are conducted at 0K which neglect thermal effects involving fluctuations in the chelator and surrounding solvent molecules.

In this work, we investigate the stability of two different Zr^{4+}-chelator complexes in aqueous solution by means of Molecular Dynamics (MD) simulations which allow for a realistic sampling of both the conformational fluctuations of the chelator and the solvent environment. Specifically, the MD simulations allow for exploring the thermodynamics of the chelating complex where the solvent and temperature effects are included in a realistic manner. The two considered chelators are Deferoxamine-B (DFO)[23] and 4HMS[1](N1,N5,N10,N14-tetra(N-hydroxy-N-methyl-1,4-dioxo-5-azapentyl)-1,5,10,14-tetraazatetradecane) which has recently been proposed in the literature[1] as a potential chelator of Zr^{4+} due to the presence of eight coordination sites. DFO and 4HMS are schematically shown in the left and right panels of Fig. 1. The metal binding ability of these two chelators is heavily influenced by their hydroxamate groups highlighted in red in Fig. 1. DFO has three hydroxamate groups allowing in principle, six oxygen atoms for coordination with Zr^{4+}. On the other hand, 4HMS has four hydroxamate groups increasing the possible coordination with Zr^{4+} to eight.

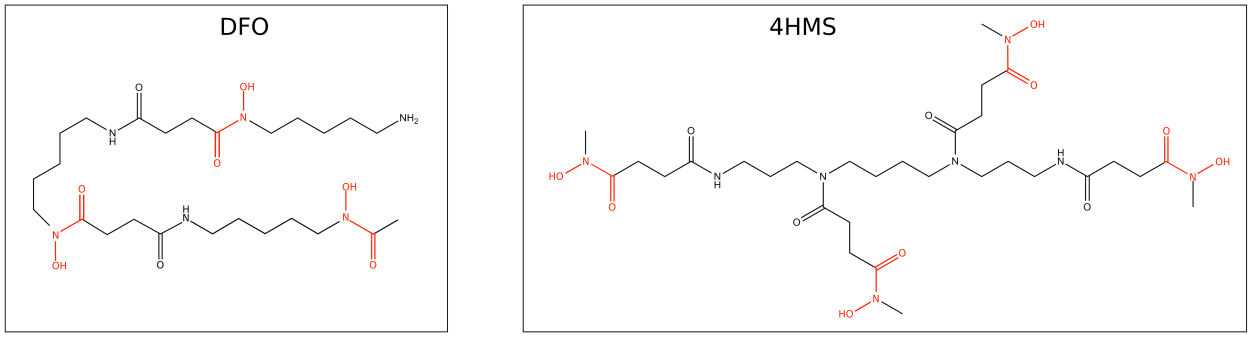

Figure 1: Schematic representation of DFO and 4HMS chelators. Hydroxamate groups of both molecules are highlighted in red.

Results

Free Energy Landscape of Zr^{4+}-DFO Complex in Solvent

We first performed a $1\mu sec$ MD simulation of Zr^{4+}-DFO complex in water at room temperature, choosing as the initial configuration, the DFT optimized structure from Ref. 22 with six-fold coordination. This structure was then solvated with over 3000 water molecules and subject to energy minimization. Besides the six-fold coordination involving the hydroxamate groups, two coordinating trans-oriented oxygen atoms from water molecules were found in our optimized structure, consistent with the findings of Holland and co-workers.[22] Starting from this minimized structure, we initiated molecular dynamics simulations at 300K. In order to track the dynamic evolution of the hydroxamate groups coordinating the Zr^{4+} we built a variable, CN, mathematically defined in equation 3 in the Methods section, which essentially *counts* the number of oxygen atoms belonging to the DFO hydroxamate groups that are coordinated to Zr^{4+}. Note that CN does not include oxygen atoms arising from coordinating water molecules which will be addressed separately. In this way, the CN can be used to quantify changes in the contribution of the hydroxamate groups to the first coordination sphere of the Zr^{4+} cation over the course of the molecular dynamics simulation.

The top panel of Fig. 2 shows the temporal evolution of the coordination number (CN)

for the first $200ns$ of the simulation. In the DFT-optimized structure, for example, the CN is $\simeq 6$; the bottom-left panel of Fig. 2 shows that in this structure the Zr^{4+} is surrounded by the three hydroxamate groups in the stable complex. At the beginning of the simulation, the CN oscillates around a value of 5.5. This initial value differs by 0.5 from the coordination observed in the DFT structure as a consequence of small modifications of the DFO structure occurring during the equilibration phase of the system (see Methods section). One might interpret this as a fluctuation between bidentate and monodentate binding of the hydroxamate oxygen atoms to the Zr^{4+} cation.

The time series of the CN (upper panel of Fig. 2) shows that there is a transition from $CN \simeq 5.5$ to $CN \simeq 3.5$ at $\sim$ 2ns. This transition is irreversible; the CN never reverts back to the original value for the rest of the simulation lasting approximately 200ns. The bottom-right panel of Fig. 2 represents the snapshot of the simulation at 200ns. The structure of the complex indicates a fewer number of DFO oxygen atoms involved in Zr^{4+} complexation. The fact that the hydroxamate group closest to the NH_3 terminus has moved away from the inner Zr^{4+} coordination sphere, suggests that, although the initial configuration (DFT-optimized structure) is likely to be the most stable structure on the potential energy landscape relevant at 0K, its stability is altered by both temperature and water.

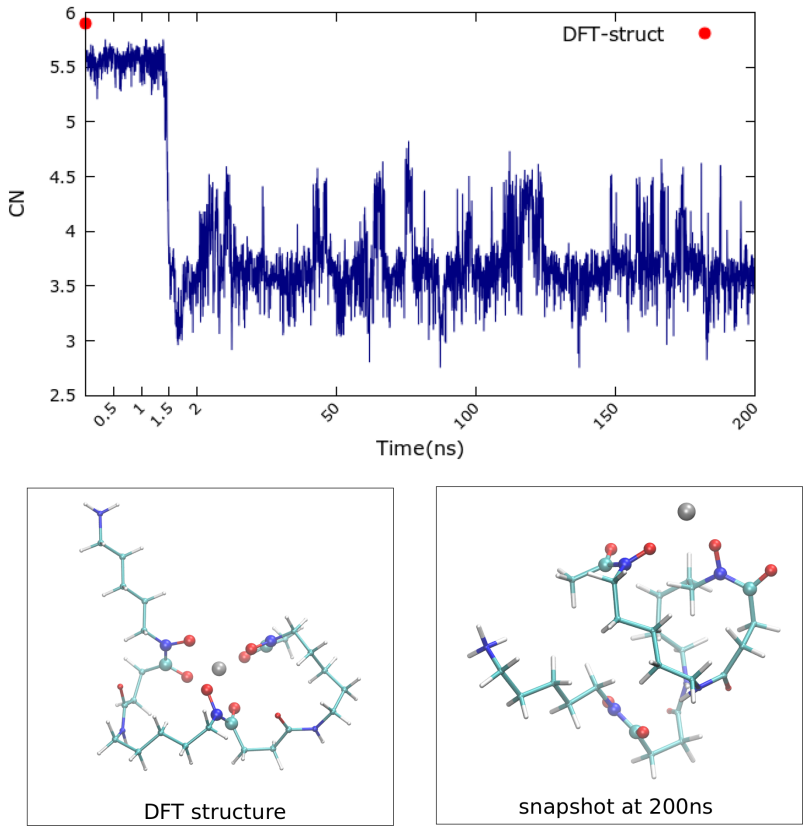

Figure 2: Upper panel: temporal evolution of the CN collective variable, along the first 200ns, of the simulation of the Zr^{4+}-DFO complex in water. Bottom-Left panel: DFT structure of the Zr^{4+}-DFO complex, from Ref. 22 (without water molecules). Bottom-Right panel: a snapshot of the simulation after 200ns. For both bottom panels, the red highlighted atoms are the ones belonging to the hydroxamate groups.

We turned to construct the free energy landscape of the Zr^{4+}-DFO complex to better understand the results in Fig.2 where there are no events where the initial structure is re-visited on the timescale of hundreds of nanoseconds. Therefore, one cannot reliably construct the correct Boltzmann weighted probabilities of the configurations in order to determine relative free energies of different conformational states. To circumvent this problem, we focused on examining the free energy profile along the CN using the umbrella sampling technique.[24] The principle behind this method is that one adds an external potential to the system in order to achieve a non-Boltzmann sampling of regions that are poorly explored, which can be subsequently re-weighted to determine the correct free energy of the system.[24–26]

In detail, we performed a series of $1\mu sec$ long MD simulations of the Zr^{4+}-DFO complex

in water, in which a harmonic biasing potential is put on the CN at different values. In total, we generated approximately $9\mu sec$ of simulations for our analysis. All the simulations have the same value of the harmonic constant ($k = 20k_BT$), but differ in the value of the center of the harmonic potential (centers go from $CN = 2$ to $CN = 6$, with a 0.5 step). This means that in each simulation, we are forcing (biasing) a specific number of coordinating hydroxamate oxygen atoms, given by the value of the center of the bias. The FES is then reconstructed from the probability distribution of the CN obtained from each of these *biased* simulations, using the WHAM method[27,28] (code from Ref. 29).

The top panel of Fig. 3 shows the FES we obtain for the Zr^{4+}-DFO complex along the CN coordinate. As a visual guide for the reader, the solid red vertical line shows the magnitude of the CN obtained from our initial optimized structure. Also shown, are error bars in the FES, constructed using the Monte Carlo bootstrap method,[30] as implemented in Ref. 29. Rather strikingly, we observe that the DFT-optimized structure does not correspond to the global free energy minimum, but is rather high up in energy indicating that, at room temperature, the six-fold coordination in DFO is highly unstable by at least $20k_BT$. The global minimum of the FES is observed at $CN \sim 3.5$, meaning that there are three to four oxygen atoms of DFO coordinated to Zr^{4+}.

The bottom panels of Fig. 3 visually depict representative snapshots obtained along different regions of the FES. The central structure corresponds to $CN \simeq 3.6$ (the global minimum of the FES) where only two of the three hydroxamate functional groups of DFO interact with Zr^{4+}. This illustrates that the rest of the molecule involving the N-terminus is not involved in the chelation complex. The rightmost structure of Fig. 3 corresponds to $CN \simeq 5$, with the three hydroxamate groups surrounding the Zr^{4+} cation as in the DFT structure. This complex is higher up in free energy. As we will see below, finite temperature alters the conformational fluctuations of the DFO molecule as well as the hydrogen bonds between the hydroxamate groups and the water molecules which in turn affect the binding mechanisms.

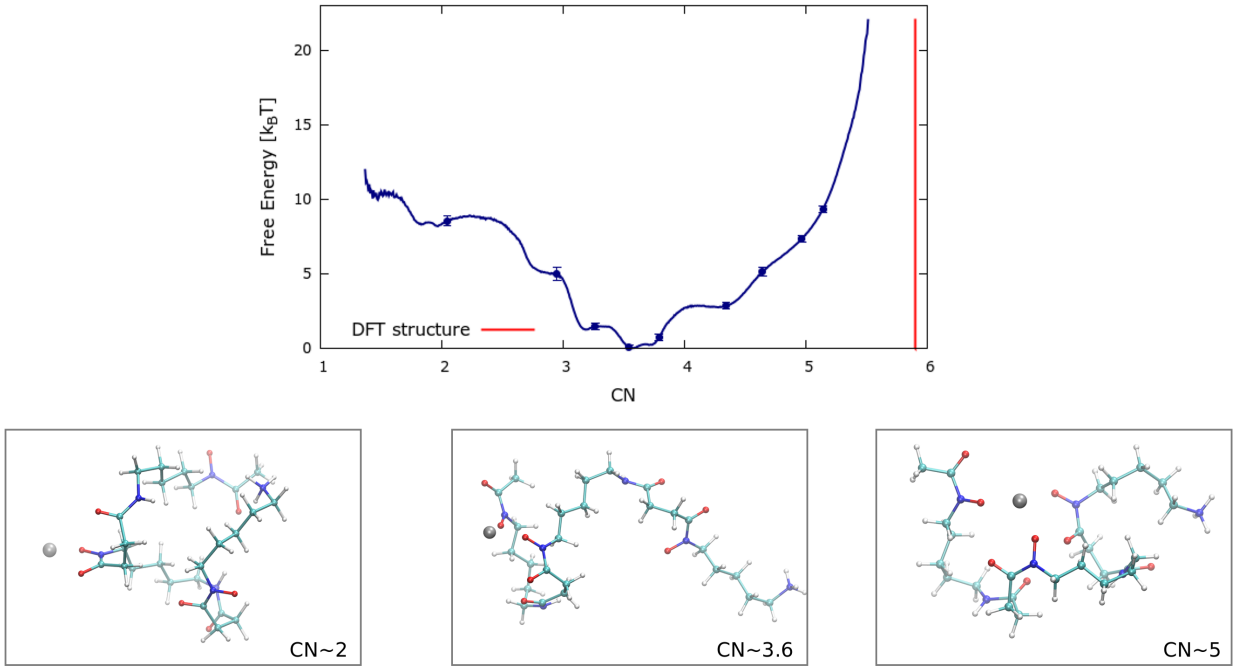

Figure 3: Upper panel: Free energy landscape of the Zr^{4+}-DFO complex in water, as a function of the CN. The red line shows the magnitude of the CN for the DFT-optimized structure from Ref. 22. Lower panels: representative conformations of the same complex, corresponding to different CN values.

Potential Energy landscape of Zr^{4+}-DFO complex

As eluded to earlier, several studies using DFT-based optimizations showed that the most stable 1:1 Zr^{4+}-DFO complex is with six oxygen atoms stemming from the DFO molecule coordinated to Zr^{4+}.[17,21,22] Our results, however, paint a different picture when temperature and solvent are explicitly included. One the one hand, there have been numerous studies of molecular systems (regarding for example the binding between ligands and proteins) showing that both solvent and temperature can have a drastic effect on both the binding mechanisms and subsequently thermodynamics.[31–37] Specific solvation of water in response to the presence of a solute such as a hydrophobic moiety or a dipole or charge re-distribution is known to play a critical role in a wide range of physical and chemical processes.[38–41] At the same time, we do not explicitly include electronic effects in our model.

In order to understand the origins of these effects better and to explore the topography

of the underlying potential energy landscape (PES), we conducted an inherent structure analysis.[42,43] This procedure has first been used to study the potential energy landscape of liquids[43–45] and soft-matter systems such as proteins.[46–48] The top panel of Fig. 4 shows a schematic of how this is conducted for our specific system. Here, we performed a geometry optimization of many structures sampled from the FES at 300K (top panel of Fig. 4), that start from different initial values of the CN. These configurations are subsequently quenched via a geometry optimization on the PES (middle panel of Fig. 4).

To allow for a more direct comparison with the conditions in previous DFT simulations, all the water molecules are removed and then the total potential energy (U) is optimized. The optimization is performed by the steepest descent method[49,50] followed by the application of the conjugate gradient algorithm.[51] The combination of these two techniques allows for the identification of the nearest minimum of U for each starting structure. A threshold of $10 \cdot 10^{-5} k_B T/\text{Å}$ is used for convergence of the forces.

The bottom panel of Fig. 4 shows a scatter plot of U vs CN obtained for all the optimized structures. We observe that the optimized geometries on the PES localize to two regions corresponding to $CN \simeq 4$ and $CN \simeq 6$. The global minimum of U is for $CN \simeq 6$, which is several $100\text{k}_B\text{T}$ lower than the other coordination configurations. These results are fully consistent with previously reported DFT calculations[22] and confirm that the differences we observe between the PES and FES arise from temperature-induced conformational disorder and solvent effects. Furthermore, the agreement with the DFT suggests that our interaction potential is sufficiently accurate to capture the structure of the chelator complex.

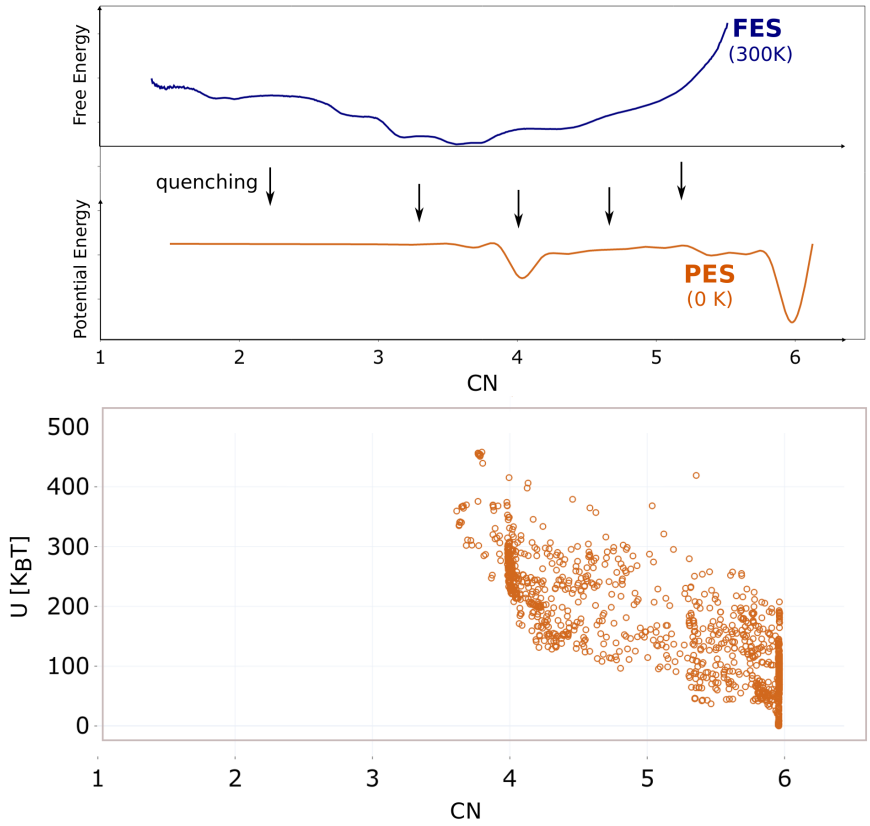

Figure 4: Top panel: schematic representation of the geometry optimization procedure. Many initial configurations are taken from different regions of the FES, quenching them in vacuum, and at 0K the resulting PES has a completely different profile. Bottom panel: Potential Energy(U) vs CN for all optimized conformations of the Zr^{4+}-DFO complex.

Comparing Free Energy Landscape of DFO and 4HMS

In a recent study, Alnahwi and co-workers showed that the 4HMS chelator presented improved chelating properties.[1] Specifically, they found using both in vitro and in vivo studies, that the molar activity of 4HMS complexed with Zr^{4+} is at least three times higher than that of DFO. In addition, by performing DFT calculations, they demonstrated that all of the eight oxygen atoms belonging to the four hydroxamate groups are bound to the Zr^{4+}, with a distance less than 2.4Å.

In order to compare the free energy landscapes for DFO and 4HMS, we repeated our umbrella sampling simulations of 4HMS, using again the CN as a collective variable. The

harmonic constant chosen was $k = 20k_BT$ with the centers of the constraints going from $CN = 2$ to $CN = 8$ using a 0.5 step. The total accumulated length of these MD simulations was $11\mu sec$. Fig. 5 compares the FES of the Zr^{4+}-DFO complex (left panel) with that for Zr^{4+}-4HMS (right panel). The FES for the two systems are strikingly different and confirm the experimental observations of the greater efficacy of 4HMS as a chelator compared to DFO. Specifically, the free energy minimum of 4HMS corresponds to a structure where all the four hydroxamate groups envelop the Zr^{4+}. For example, configurations at $CN \simeq 3.5$, which is the most stable value for DFO, are now $\simeq 35k_BT$ higher in free energy than the global minimum in 4HMS. Thus, in sharp contrast to what is observed for DFO, higher CN are more favored than lower ones fully consistent with the experimental observations.[1]

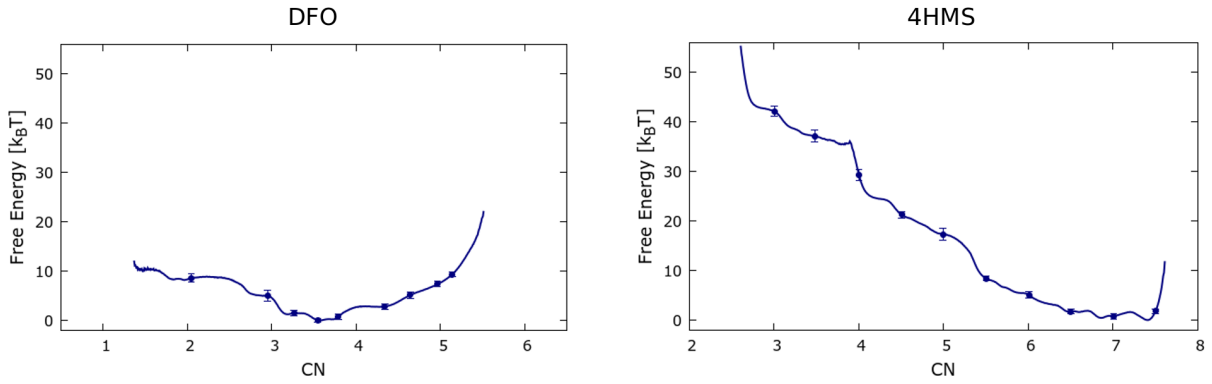

Figure 5: Left panel: Free energy profile of the Zr^{4+}-DFO complex in solvent as a function of the CN collective variable. Right panel: the same for Zr^{4+}-4HMS complex.

Conformational Heterogeneity: DFO versus 4HMS

The preceding results indicate that there are some important differences in the manner in which the hydroxamate groups of DFO and 4HMS envelope the Zr^{4+} ion. In order to quantify these differences, we examined the orientation of the hydroxamate groups relative to the Zr^{4+} ion, specifically in the free energy minima of DFO and 4HMS. For both systems, we considered two angles for each hydroxamate group: one formed by Zr^{4+}-Oxygen-Nitrogen and another formed by Zr^{4+}-Oxygen-Carbon, as depicted in the top panel of Fig. 6. In DFO, (bottom left panel of Fig. 6), there are three groups correspondingly color-coded, with each

group yielding two angles, while in 4HMS, (bottom right panel of Fig. 6), there are four groups.

The top left and top right panels of Fig. 6 show scatter plots of the two angles for DFO and 4HMS, respectively, obtained from independent configurations sampled along the trajectory at the position of the free energy minimum. The colors correspond to different hydroxamate groups (group1-group3 for DFO and group1-group4 for 4HMS). Above and on the right side of each scatter plot, the probability distributions of the corresponding angles are also shown. In the case of DFO, we see that the angular distributions of group1 and group2 (the ones interacting with Zr^{4+}) are similar; for both groups, the peaks of the probability distributions are located at $\simeq$ 1.5 radians for Zr^{4+}-O-C angles and at $\simeq$ 2.8 radians for Zr^{4+}-O-C angles. Note that the peak positions do not correspond to the angles of the DFT-optimized structure (shown as a solid green circle in the left panel). On the other hand for group3, which doesn't interact directly with Zr^{4+}, the distributions are flat, highlighting that this part of the DFO molecule has no preferred group-orientation. Since this group is next to a positively charged ammonium group, it prefers to be solvated and this, in turn, is more favorable than binding with the Zr^{4+}.

In contrast, 4HMS presents a rather different situation. Overall, we observe that all four groups are constrained to a preferred orientation which allows for a stable dipole-charge interaction to form between the chelator hydroxamate groups and Zr^{4+}. While there are some differences among the angular distributions of different groups, the peaks are localized in two defined regions ranging from one to two radians in the Zr^{4+}-O-N angles and from two to three radians in the Zr^{4+}-O-C angles.

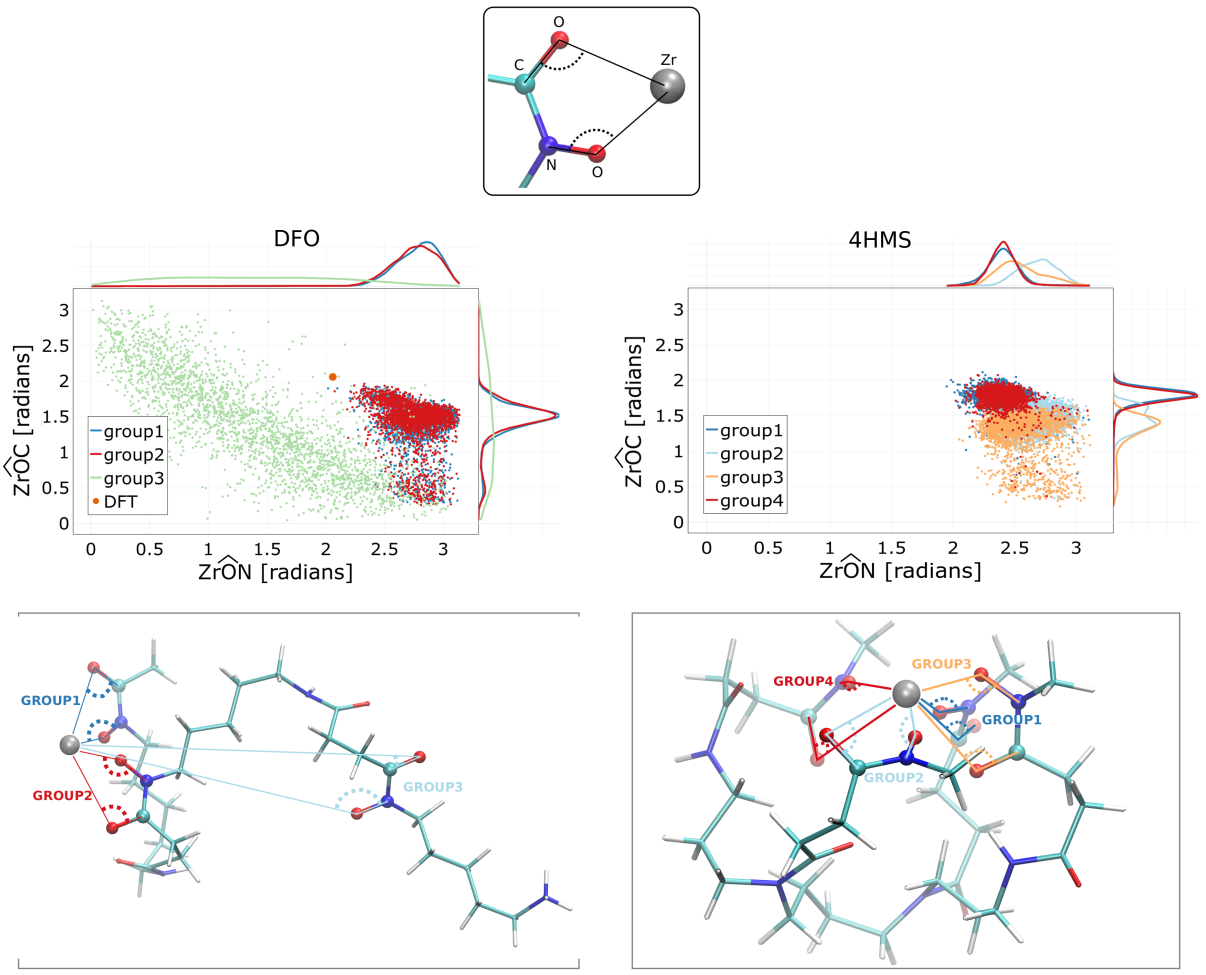

Figure 6: Top Left panel(DFO): scatter plot of the Zr^{4+}-O-N and Zr^{4+}-O-C angles (O, N, and C atoms belonging to the three hydroxamate groups of DFO). The analyzed conformations belong to the 1 μs trajectory at the free energy minimum (center of the bias at $CN = 3.5$). Top Right panel(4HMS): same scatter plot but for Zr^{4+}-O-N and Zr^{4+}-O-C angles of the four 4HMS hydroxamate groups. The conformation belongs to the 1 1 μs trajectory with the center of the bias at $CN = 7.5$. Lower panels: the angles considered are highlighted in snapshots of the analyzed trajectories.

Role of Water in Coordination Chemistry

As mentioned above, the binding mechanism of Zr^{4+} to the chelators in water will naturally involve solvation and de-solvation processes. Several of the previous DFT-based calculations have shown, by the inclusion of a few coordinating water molecules, that specific interactions with the solvent can be an important determinant in binding.[17,21,22] To understand the role of the solvent, we examined the water coordination around Zr^{4+} for both the DFO and 4HMS

chelation complex.

The Zr^{4+} aquo species has been experimentally determined in acidic aqueous solution by means of extended X-ray absorption fine structure (EXAFS) and shown to be coordinated with eight water molecules in the first coordination shell, with the bound oxygen atoms located at an average distance of $\simeq$2.2Å.[52] Upon binding of the chelate, the number of water molecules changes depending on the number of hydroxamate groups that become coordinated with the ion. To understand the magnitude of this change, we conducted a 200ns MD simulation of an isolated Zr^{4+} in bulk water. The number of water molecules coordinating the Zr^{4+} was then compared to that obtained from the free energy minimum of the chelator complex.

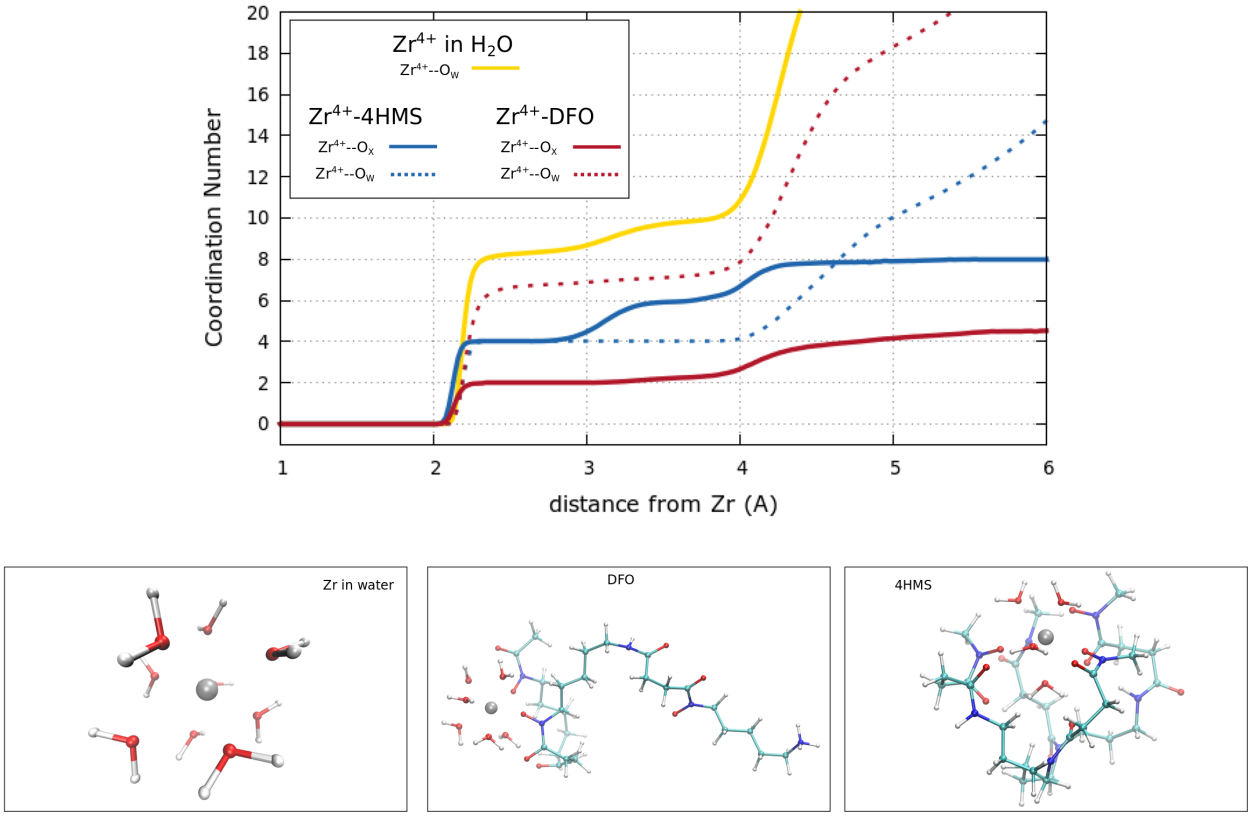

Figure 7: Upper panel: Coordination number of oxygen atoms around Zr^{4+} as a function of distance from the ion. The solid yellow line refers to the simulation of Zr^{4+} in bulk water. Blue lines refer to the simulation of Zr^{4+}-4HMS in water, whereby the solid line shows the number of hydroxamate oxygen atoms of 4HMS, and the dotted line shows the number of coordinating water molecules. Red lines refer to the simulation of Zr^{4+}-DFO again with the solid line depicting the number of DFO hydroxamate oxygen atoms coordinating Zr^{4+} and the dotted line the number of water molecules. Lower panels: Representative structures from the analyzed simulations, showing only water molecules whose oxygen atoms lie within a distance of 2.3Å.

In Fig. 7, the coordination numbers of Zr^{4+}, as a function of the distance of oxygen atoms from the ion, are shown. These plots show regions where there are sharp changes in the coordination followed by plateaus which essentially correspond to different solvation shells. In the case of Zr^{4+} aquo species (yellow line), the number of coordinating water molecules grows to ∼8 between 2.0Å to 2.5Å, in agreement with experimental reports[52] (see a representative snapshot from simulations in the bottom left panel of Fig. 7). As expected, these numbers change for Zr^{4+}-DFO and Zr^{4+}-4HMS simulations. In the case of the Zr^{4+}-DFO complex,

two oxygen atoms from the DFO hydroxamate groups and six oxygen atoms from water are coordinated to Zr^{4+} in the range from 2.2Å to 3Å. Thus, the Zr^{4+} remains almost fully solvated when complexed with DFO (see a representative snapshot from simulations bottom middle panel of Fig. 7).

Interestingly, for the case of Zr^{4+}-4HMS at distances less than 3.0Å, the ion appears to be equally coordinated to four oxygen atoms from 4HMS and four oxygen atoms from surrounding water molecules (see a representative snapshot from simulations bottom right panel of Fig. 7)). Similar to DFO, the reduced coordination from the chelator hydroxamate groups originates from the fact that, unlike at 0-K, the oxygen atoms of the hydroxamate groups do not symmetrically coordinate the ion which subsequently leads to differences in the Zr^{4+}-O-N and Zr^{4+}-O-C angles. Beyond 3.0Å, the coordination around the Zr^{4+} increases from 4 to $\sim$8 originating solely from the oxygen atoms of the hydroxamate groups. Our results, therefore, suggest that the competition between the hydroxamate groups versus specific water molecules in fulfilling Zr^{4+} coordination sphere can have non-trivial effects in either forming unstable (DFO) or stable complexes (4HMS).

Given the prominent role of the changes in water solvation around the Zr^{4+} upon binding to DFO and 4HMS, it is interesting to understand whether this has any impact on the thermodynamics reported in Fig. 5. Specifically, the free energy curves discussed earlier are along one reaction coordinate only, namely the CN collective variable which counts the oxygen atoms belonging to the chelator hydroxamate groups coordinating the ion. From the 1-dimensional umbrella sampling simulations, it is also possible to reconstruct a 2-dimensional free energy surface along our original CN variable and another variable that counts the number of water molecules coordinating the Zr^{4+} (labeled as $CN_{Zr^{4+}--O_W}$, see Methods section for definition). Fig. 8 shows the 2-dimensional free energy surfaces constructed for DFO (left panel) and 4HMS (right panel) as a function of the original CN we used earlier (labeled as $CN_{Zr^{4+}--O_X}$ on the x-axes) and of the $CN_{Zr^{4+}--O_W}$ (on the y-axes) . For both DFO and 4HMS, we observe that explicit inclusion of solvation in the reaction coordinate

does not change our conclusions. For DFO, the free energy minimum involves a structure where there are three to four oxygen atoms of DFO coordinated to Zr^{4+} while for 4HMS, the minimum occurs approximately at 8 hydroxamate oxygen atoms. Furthermore, the free energy differences between the stable and high energy structures are also consistent between the 1-d and 2-d analyses.

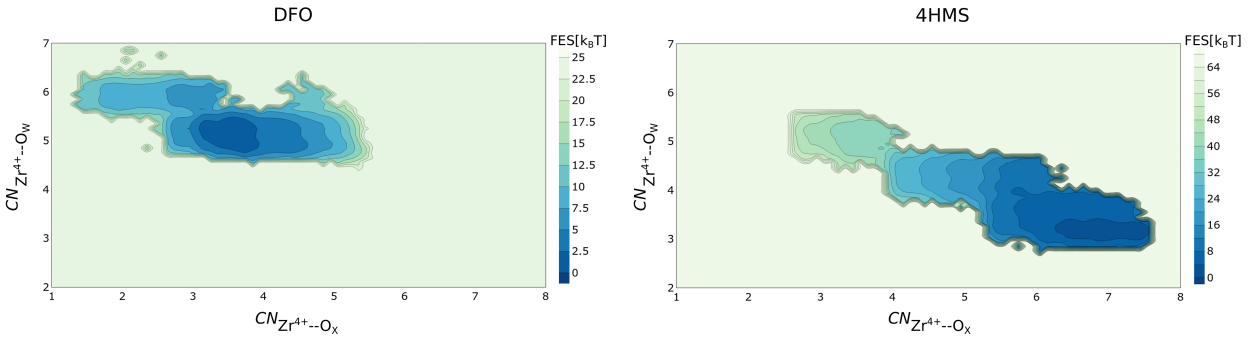

Figure 8: Left panel: Free energy landscape of the Zr^{4+}-DFO complex in solvent as a function of the oxygen atoms belonging to the hydroxamate groups coordinating the ion (x-axes) and of oxygen atoms from surrounding water coordinating the ion (y-axes). See section methods for mathematical definitions of the two collective variables. Right panel: the same for Zr^{4+}-4HMS complex.

.

Discussion and Conclusions

In the last decade, there has been a spurt of research activity in the field of radionuclide science searching for optimized chelating molecules as anchors for radioisotopes in radiopharmaceutical development, including Zirconium-89 (^{89}Zr). Identifying optimal chelating compounds has enormous potential in radio-diagnostic and radiotherapy applications. One of the most popular chelators that has been the subject of several experimental and theoretical studies is DFO. Despite its wide usage, improving its efficacy in-vivo has prompted the design of DFO-like chelators with enhanced coordination with Zirconium. It thus appears timely to harness advanced theoretical tools to guide the design and development of such systems.

The vast majority –if not all– of theoretical work to date, addressing the coordination

chemistry of Zirconium and potential chelators has been informed by DFT-based electronic structure calculations. While this approach provides a more accurate treatment of the electronic induced forces between the nuclei, thermal effects and the role of solvation are neglected. In this work, we have used classical molecular dynamics simulations of Zr^{4+} in water to examine the thermodynamics of the chelating complex for two chelators namely DFO and 4HMS. Our findings paint a more complex scenario than that observed in previous DFT calculations. Specifically, the DFT-optimized structure, in which the three hydroxamate groups of DFO enclose Zr^{4+}, is not stable in the MD simulations. Free energy calculations instead show that the most stable Zr^{4+}-DFO configuration has only two oxygen atoms from DFO coordinated to the cation. Furthermore, water oxygen atoms have a prominent role in filling the ion's first coordination shell.

For 4HMS, we find that the octacoordinated complex is thermodynamically stable at room temperature and in the presence of solvent molecules, with all four hydroxamate groups enclosing the ion. These results highlight the importance of both specific solvation of water molecules and the orientation of the hydroxamate groups relative to the Zr^{4+} in stabilizing the Zr^{4+}-4HMS complex. We believe that these molecular insights informed by computational studies, offer important design principles that could motivate and guide the experimental search for better Zirconium chelators.

Computational Methods

For both DFO and 4HMS, we study the case of deprotonated molecule where all hydrogens bound to the oxygen atoms of the hydroxamic acid are removed. From experimental acidity constants,[23] we know that DFO in water at neutral pH has completely protonated hydroxamic groups and the NH_3^+ terminal is also protonated. Highly charged Zr^{4+} has a high affinity for hard Lewis bases and complexes stepwise with DFO under deprotonation of the hydroxyl of the hydroxamate group already starting at pH 2. The DFO molecule, with a

positively charged ammonium group, has thus a total charge of -2, whereas the deprotonated 4HMS molecule has a total charge of -4, as it has no -NH_2 terminus.

The GAFF Force Field[53] for organic molecules, was used to construct interaction potentials for the DFO and 4HMS molecules through the Antechamber package.[54] The charges are calculated using the AM1-BCC charge model.[55] The chelator molecules are solvated with 3667 and 3410 water molecules for the DFO and 4HMS molecules respectively, using the single point charge (SPC/E) water model.[56] This water model is rigid-body and non-dissociable and therefore speciation events for example between Zirconium and waters ionic products coming from hydrolysis are not taken into account.[57] In recent years, Mertz and co-workers have shown that in order to obtain both accurate structural and thermodynamic properties associated with the binding of transition metal ions to proteins, classical force fields can be corrected via the inclusion of an extra attractive term[58] ($\propto \frac{1}{r^4}$) which leads to the following non-bonded interaction potential shown below.

$$U_{ij} = \frac{e^2 Q_i Q_j}{r_{ij}} - \frac{c_4^{ij}}{r_{ij}^4} + \frac{c_{12}^{ij}}{r_{ij}^{12}} - \frac{c_6^{ij}}{r_{ij}^6} \tag{1}$$

The extra term ($\propto \frac{1}{r^4}$) mimics charge–induced dipole interactions. The force field parameters for Zr^{4+} ion are taken from Ref. 58.

All the MD simulations are run using the Amber2020 package. The Zr^{4+}-chelate complexes are placed in a cubic box of water, where the closest distance between the complex and the box wall was 17Å. In the case of DFO, two chloride ions are added to neutralize the system. For both systems, we conduct an equilibration procedure before moving to production runs. Firstly a minimization step is performed, then the temperature is gradually brought from 0K to 300K along an NVT simulation of 20 ps, and finally, the density is equilibrated through a simulation in the NPT ensemble for 2 ns using the Berendsen barostat[59] fixed at 1 bar. This equilibration phase is followed by a $1\mu s$ simulation in the NVT ensemble at a temperature of 300K. The box size for DFO along the x, y and z are 59.9 Å, 51.7 Å and 46.9 Å respectively, while for 4HMS it is 53.8 Å, 53.1 Å and 48.1 Å. In all the MD

simulations, the time step is set to 2 fs where the temperature is controlled using a Langevin thermostat[60] using a time constant of $\gamma = 2ps^{-1}$. A cutoff of 11 Å is used for the non-bonded interactions. Long-range corrections to the van-der-Waals are included. The Particle Mesh Ewald (PME)[61] is used to treat the long-range part of the Coulomb interactions.

To study the ion-chelator coordination chemistry, we choose as a collective variable the coordination number between Zr^{4+} and the oxygen atoms belonging to the hydroxamate groups of the chelator, defined as:

$$CN = \sum_i \frac{1 - (\frac{d_i}{r_0})^6}{1 - (\frac{d_i}{r_0})^{12}} \tag{2}$$

The index i runs over the oxygen atoms belonging to the hydroxamate groups of the chelator (6 in the DFO case, 8 in the 4HMS case), d_i is the distance between i-oxygen and Zr^{4+}, $r_0 = 5$Å is the cut-off parameter of the switching function.

As described in the Results, we used the Umbrella Sampling technique[24] to reconstruct the free energy landscape of the Zr^{4+}-DFO and Zr^{4+}-4HMS complex in solvent as a function of the CN. These constrained simulations were obtained using the Amber suite combined with tools from PLUMED open source library.[62] The free energy landscapes are then reconstructed using the WHAM method (code from Ref. 29.)

To study the ion-water coordination chemistry, we defined a second collective variable that counts the number of oxygen atoms from surrounding water molecules coordinating Zr^{4+}:

$$CN_{Zr^{4+}--O_W} = \sum_i \frac{1 - (\frac{d_i}{r_0})^{10}}{1 - (\frac{d_i}{r_0})^{20}} \tag{3}$$

The index i runs over the oxygen atoms belonging to all water molecules, d_i is the distance between i-oxygen and Zr^{4+}, $r_0 = 2.5$Å is the cut-off parameter of the switching function. The 2-dimensional free energy landscapes are also obtained using the WHAM method (code from Ref. 29.)

Acknowledgements

A.A.H. acknowledges funding by the European Union (ERC, HyBOP, Grant Number: 101043272). Views and opinions expressed are however those of the author(s) only and do not necessarily reflect those of the European Union or the European Research Council. Neither the European Union nor the granting authority can be held responsible for them.

References

(1) Alnahwi, A. H.; Ait-Mohand, S.; Dumulon-Perreault, V.; Dory, Y. L.; Guerin, B. Promising Performance of 4HMS, a New Zirconium-89 Octadendate Chelator. ACS omega **2020**, 5, 10731–10739.

(2) Kunos, C. A.; Mankoff, D. A.; Schultz, M. K.; Graves, S. A.; Pryma, D. A. Radiopharmaceutical Chemistry and Drug Development-What's Changed? Semin Radiat Oncol **2021**, 31, 3–11.

(3) Witney, T. H.; Blower, P. J. The chemical tool-kit for molecular imaging with radionuclides in the age of targeted and immune therapy. Cancer Imaging **2021**, 21, 18.

(4) Kraeber-Bodéré, F.; Rousseau, C.; Bodet-Milin, C.; Mathieu, C.; Guérard, F.; Frampas, E.; Carlier, T.; Chouin, N.; Haddad, F.; Chatal, J.-F. et al. Tumor Immunotargeting Using Innovative Radionuclides. International Journal of Molecular Sciences **2015**, 16, 3932–3954.

(5) Deri, M. A.; Zeglis, B. M.; Francesconi, L. C.; Lewis, J. S. PET imaging with 89Zr: From radiochemistry to the clinic. Nuclear Medicine and Biology **2013**, 40, 3–14.

(6) Clinical trial.gov accessed Dec 2022. `https://clinicaltrials.gov/`.

(7) Cyclotron Produced Radionuclides: Physical Characteristics and Production Methods; Nr.468 Technical reports series. International Atomic Energy Agency, 2009.

(8) Production of Zirconium-89 and the Development of Zr-89 Radiopharmaceuticals. https://www.iaea.org/projects/crp/f22071.

(9) Meijs, W. E.; Herscheid, J. D.; Haisma, H. J.; Pinedo, H. M. Evaluation of desferal as a bifunctional chelating agent for labeling antibodies with Zr-89. International Journal of Radiation Applications and Instrumentation. Part A. Applied Radiation and Isotopes **1992**, 43, 1443–1447.

(10) Baroncelli, F.; Grossi, G. The complexing power of hydroxamic acids and its effect on the behaviour of organic extractants in the reprocessing of irradiated fuels—I the complexes between benzohydroxamic acid and zirconium, iron (III) and uranium (VI). Journal of Inorganic and Nuclear Chemistry **1965**, 27, 1085–1092.

(11) Meijs, W. E.; Herscheid, J. D.; Haisma, H. J.; Pinedo, H. M. Evaluation of desferal as a bifunctional chelating agent for labeling antibodies with Zr-89. International journal of radiation applications and instrumentation. Part A. Applied radiation and isotopes **1992**, 43, 1443–1447.

(12) Feiner, I. V.; Brandt, M.; Cowell, J.; Demuth, T.; Vugts, D.; Gasser, G.; Mindt, T. L. The race for hydroxamate-based zirconium-89 chelators. Cancers **2021**, 13, 4466.

(13) Wang, Z.; Qiu, W.; Pang, S.; Jiang, J. Effect of chelators on the production and nature of the reactive intermediates formed in Fe(II) activated peroxydisulfate and hydrogen peroxide processes. Water Research **2019**, 164, 114957.

(14) Ulvenlund, S.; S. Georgopoulou, A.; Michael P. Mingos, D.; Baxter, I.; E. Lawrence, S.; J. P. White, A.; J. Williams, D. Synthesis and characterisation of chelating polycarboxylate ligands capable of forming intermolecular, complementary triple hydrogen bonds. J. Chem. Soc., Dalton Trans. **1998**, 1869–1878.

(15) Deri, M. A.; Zeglis, B. M.; Francesconi, L. C.; Lewis, J. S. PET imaging with 89Zr: from radiochemistry to the clinic. Nuclear medicine and biology **2013**, 40, 3–14.

(16) Abou, D. S.; Ku, T.; Smith-Jones, P. M. In vivo biodistribution and accumulation of 89Zr in mice. Nuclear medicine and biology **2011**, 38, 675–681.

(17) Savastano, M.; Bazzicalupi, C.; Ferraro, G.; Fratini, E.; Gratteri, P.; Bianchi, A. Tales of the unexpected: the case of zirconium (iv) complexes with desferrioxamine. Molecules **2019**, 24, 2098.

(18) Savastano, M.; Boscaro, F.; Bianchi, A. Metal Coordination Properties of a Chromophoric Desferrioxamine (DFO) Derivative: Insight on the Coordination Stoichiometry and Thermodynamic Stability of Zr4+ Complexes. Molecules **2022**, 27, 184.

(19) Imura, R.; Ida, H.; Sasaki, I.; Ishioka, N. S.; Watanabe, S. Re-Evaluations of Zr-DFO Complex Coordination Chemistry for the Estimation of Radiochemical Yields and Chelator-to-Antibody Ratios of 89Zr Immune-PET Tracers. Molecules **2021**, 26, 4977.

(20) Toporivska, Y.; Gumienna-Kontecka, E. The solution thermodynamic stability of desferrioxamine B (DFO) with Zr (IV). Journal of Inorganic Biochemistry **2019**, 198, 110753.

(21) Holland, J. P. Predicting the thermodynamic stability of zirconium radiotracers. Inorganic chemistry **2020**, 59, 2070–2082.

(22) Holland, J. P.; Divilov, V.; Bander, N. H.; Smith-Jones, P. M.; Larson, S. M.; Lewis, J. S. 89Zr-DFO-J591 for immunoPET of prostate-specific membrane antigen expression in vivo. Journal of Nuclear Medicine **2010**, 51, 1293–1300.

(23) Bellotti, D.; Remelli, M. Deferoxamine B: A natural, excellent and versatile metal chelator. Molecules **2021**, 26, 3255.

(24) Torrie, G. M.; Valleau, J. P. Nonphysical sampling distributions in Monte Carlo free-

energy estimation: Umbrella sampling. Journal of Computational Physics **1977**, 23, 187–199.

(25) Torrie, G. M.; Valleau, J. P. Monte Carlo free energy estimates using non-Boltzmann sampling: Application to the sub-critical Lennard-Jones fluid. Chemical Physics Letters **1974**, 28, 578–581.

(26) Kästner, J. Umbrella sampling. Wiley Interdisciplinary Reviews: Computational Molecular Science **2011**, 1, 932–942.

(27) Kumar, S.; Rosenberg, J. M.; Bouzida, D.; Swendsen, R. H.; Kollman, P. A. The weighted histogram analysis method for free-energy calculations on biomolecules. I. The method. Journal of computational chemistry **1992**, 13, 1011–1021.

(28) Kumar, S.; Rosenberg, J. M.; Bouzida, D.; Swendsen, R. H.; Kollman, P. A. Multidimensional free-energy calculations using the weighted histogram analysis method. Journal of Computational Chemistry **1995**, 16, 1339–1350.

(29) Grossfield, A. WHAM: the weighted histogram analysis method. `http://membrane.urmc.rochester.edu/wordpress/?page_id=126`.

(30) Efron, B.; Tibshirani, R. J. An introduction to the bootstrap; CRC press, 1994.

(31) Biela, A.; Nasief, N. N.; Betz, M.; Heine, A.; Hangauer, D.; Klebe, G. Dissecting the hydrophobic effect on the molecular level: the role of water, enthalpy, and entropy in ligand binding to thermolysin. Angewandte Chemie International Edition **2013**, 52, 1822–1828.

(32) Krimmer, S. G.; Betz, M.; Heine, A.; Klebe, G. Methyl, ethyl, propyl, butyl: futile but not for water, as the correlation of structure and thermodynamic signature shows in a congeneric series of thermolysin inhibitors. ChemMedChem **2014**, 9, 833–846.

(33) Darby, J. F.; Hopkins, A. P.; Shimizu, S.; Roberts, S. M.; Brannigan, J. A.; Turkenburg, J. P.; Thomas, G. H.; Hubbard, R. E.; Fischer, M. Water networks can determine the affinity of ligand binding to proteins. Journal of the American Chemical Society **2019**, 141, 15818–15826.

(34) Bradford, S.; El Khoury, L.; Ge, Y.; Osato, M.; Mobley, D.; Fischer, M. Temperature artifacts in protein structures bias ligand-binding predictions. Chem Sci 12: 11275-11293. 2021.

(35) Fischer, M. Macromolecular room temperature crystallography. Quarterly Reviews of Biophysics **2021**, 54.

(36) Limongelli, V.; Marinelli, L.; Cosconati, S.; La Motta, C.; Sartini, S.; Mugnaini, L.; Da Settimo, F.; Novellino, E.; Parrinello, M. Sampling protein motion and solvent effect during ligand binding. Proceedings of the National Academy of Sciences **2012**, 109, 1467–1472.

(37) Jong, K.; Hassanali, A. A. A Data Science Approach to Understanding Water Networks Around Biomolecules: The Case of Tri-Alanine in Liquid Water. The Journal of Physical Chemistry B **2018**, 122, 7895–7906, PMID: 30019898.

(38) Bagchi, B. Dynamics of Solvation and Charge Transfer Reactions in Dipolar Liquids. Annual Review of Physical Chemistry **1989**, 40, 115–141.

(39) Ben-Amotz, D. Water-Mediated Hydrophobic Interactions. Annual Review of Physical Chemistry **2016**, 67, 617–638, PMID: 27215821.

(40) Hassanali, A. A.; Zhong, D.; Singer, S. J. An AIMD Study of CPD Repair Mechanism in Water: Role of Solvent in Ring Splitting. The Journal of Physical Chemistry B **2011**, 115, 3860–3871, PMID: 21417372.

(41) Hassanali, A. A.; Zhong, D.; Singer, S. J. An AIMD Study of the CPD Repair Mechanism in Water: Reaction Free Energy Surface and Mechanistic Implications. The Journal of Physical Chemistry B **2011**, 115, 3848–3859, PMID: 21417374.

(42) Stillinger, F. H.; Weber, T. A. Hidden structure in liquids. Physical Review A **1982**, 25, 978.

(43) Stillinger, F. H.; Weber, T. A. Dynamics of structural transitions in liquids. Physical Review A **1983**, 28, 2408.

(44) Denny, R. A.; Reichman, D. R.; Bouchaud, J.-P. Trap models and slow dynamics in supercooled liquids. Physical review letters **2003**, 90, 025503.

(45) Berthier, L.; Garrahan, J. P. Nontopographic description of inherent structure dynamics in glassformers. The Journal of chemical physics **2003**, 119, 4367–4371.

(46) Nakagawa, N.; Peyrard, M. The inherent structure landscape of a protein. Proceedings of the National Academy of Sciences **2006**, 103, 5279–5284.

(47) Kim, J.; Keyes, T. Inherent structure analysis of protein folding. The Journal of Physical Chemistry B **2007**, 111, 2647–2657.

(48) Rao, F.; Karplus, M. Protein dynamics investigated by inherent structure analysis. Proceedings of the National Academy of Sciences **2010**, 107, 9152–9157.

(49) Curry, H. B. The method of steepest descent for non-linear minimization problems. Quarterly of Applied Mathematics **1944**, 2, 258–261.

(50) Lemaréchal, C. Cauchy and the gradient method. Doc Math Extra **2012**, 251, 10.

(51) Press, W. H.; Teukolsky, S. A.; Vetterling, W. T.; Flannery, B. P. Numerical recipes 3rd edition: The art of scientific computing; Cambridge university press, 2007.

(52) Hagfeldt, C.; Kessler, V.; Persson, I. Structure of the hydrated, hydrolysed and solvated zirconium (IV) and hafnium (IV) ions in water and aprotic oxygen donor solvents. A crystallographic, EXAFS spectroscopic and large angle X-ray scattering study. Dalton Transactions **2004**, 2142–2151.

(53) Wang, J.; Wolf, R. M.; Caldwell, J. W.; Kollman, P. A.; Case, D. A. Development and testing of a general amber force field. Journal of computational chemistry **2004**, 25, 1157–1174.

(54) Wang, J.; Wang, W.; Kollman, P. A.; Case, D. A. Automatic atom type and bond type perception in molecular mechanical calculations. Journal of molecular graphics and modelling **2006**, 25, 247–260.

(55) Jakalian, A.; Jack, D. B.; Bayly, C. I. Fast, efficient generation of high-quality atomic charges. AM1-BCC model: II. Parameterization and validation. Journal of computational chemistry **2002**, 23, 1623–1641.

(56) Berweger, C. D.; van Gunsteren, W. F.; Müller-Plathe, F. Force field parametrization by weak coupling. Re-engineering SPC water. Chemical physics letters **1995**, 232, 429–436.

(57) Cho, H.-R.; Walther, C.; Rothe, J.; Neck, V.; Denecke, M. A.; Dardenne, K.; Fanghänel, T. Combined LIBD and XAFS investigation of the formation and structure of Zr (IV) colloids. Analytical and bioanalytical chemistry **2005**, 383, 28–40.

(58) Li, P.; Song, L. F.; Merz Jr, K. M. Parameterization of highly charged metal ions using the 12-6-4 LJ-type nonbonded model in explicit water. The Journal of Physical Chemistry B **2015**, 119, 883–895.

(59) Berendsen, H. J.; Postma, J. v.; Van Gunsteren, W. F.; DiNola, A.; Haak, J. R. Molecular dynamics with coupling to an external bath. The Journal of chemical physics **1984**, 81, 3684–3690.

(60) Tuckerman, M. Statistical mechanics: theory and molecular simulation; Oxford university press, 2010.

(61) Darden, T.; York, D.; Pedersen, L. Particle mesh Ewald: An N log (N) method for Ewald sums in large systems. The Journal of chemical physics **1993**, 98, 10089–10092.

(62) Promoting transparency and reproducibility in enhanced molecular simulations. Nature methods **2019**, 16, 670–673.